Chapter 5

Wide field of view off axis common path self-referencing digital holographic microscopy using low coherent source

This chapter describes the use of LED (low coherent source) as a source of light in various off axis common path self-referencing digital holographic configurations to perform quantitative phase contrast microscopy of phase objects including human RBC. As discussed in Chapter 1 and Chapter 2, a low coherent source such as LED offers many advantages such as higher signal to noise ratio, by reducing the parasitic interference noise consequently enhancing the image quality, compact configurations and exotic wavelenghts. However, owing to its low spatio-temporal coherence, the main issue that needs to be addressed is the difficulty in generating high contrast fringes over a large FOV.

5.1 Exploiting coherence properties of LEDs

Although high stability is achieved, integrating LED (quasi monochromatic source) in most of the common path self-referencing geometry is difficult owing to the fact that the path length difference in both beams does not fall within the coherence length to achieve stable interference pattern with appreciable visibility over large FOV. The low temporal coherence of LED can be enhanced by introducing appropriate spectral filters. The spatial coherence of a LED source can be enhanced by decreasing the lateral extent of the effective emitting area by using a spatial filter assembly consisting of a lens and a pinhole. However, these steps can appreciably reduce the operational intensity and there is a trade-off between the pursued degree of coherence and the usable intensity. To enhance the spatial coherence of the LED without effecting the output flux, instead of a spatial filtering assembly, a MO lens (which acts as a de-magnifying lens) (10X, NA=0.25) is used. This reduces the effective emitting area of the source, by creating a demagnified real image of the LED light emitting area. This is achieved by passing the light output from the LED source through a MO which focusses the incoming light to a point source, which expands as it travels further as shown in Fig 5.1, increasing the area of spatial coherence.

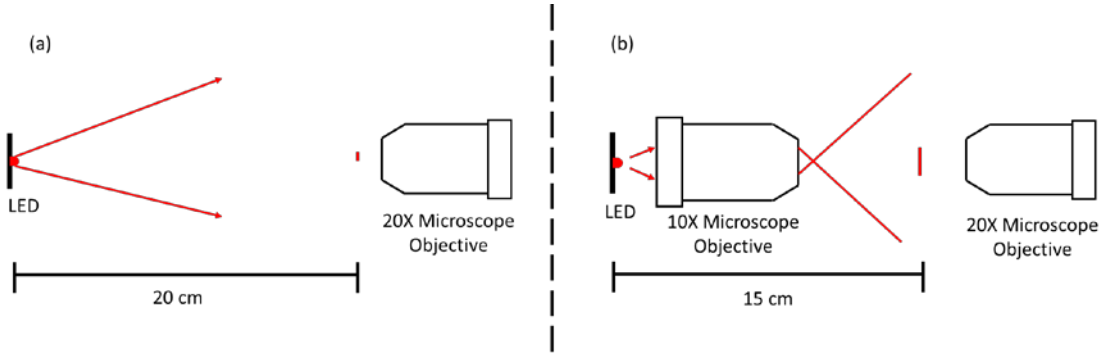

Fig 5.1 Diameter of the spatial coherence area increases upon demagnifying the light emitting area of the source.

5.2 Incorporating LED in common path self-referencing geometries

After harnessing the spatial coherence of LED, optical arrangement utilizing multiple self-referencing modules for hologram multiplexing is implemented. As a result of utilizing multiple self-referencing modules, one obtains multiple interference regions that contain object information in a single shot which consequently increases the usable FOV. The multiple spatially separated interference regions when recorded/stitched together on the same sensor array creates a large effective FOV.

After achieving a large FOV, a comparative study is undertaken with different light sources and sensors across three off axis self-referencing geometries for performing interference microscopy, namely (1) Fresnel Biprism, (2) Lloyd's mirror and (3) Sagnac interferometer. The study is undertaken to explore which combination gives the best output in terms of the cost of the system, resolution and signal to noise ratio by examining polystyrene beads and human red blood cells (RBCs).

Set of experiments are conducted using 4 different light sources:

1. UV LED (λ=385 nm, Luxeon star, max output power=475 mW, emitting area 1 mm^2)
2. Red LED (λ=627 nm, Luxeon star, max output power=2W, emitting area 1 mm^2)
3. He-Ne Laser (λ=632 nm, Thorlabs, Maximum output power<2 mW)
4. Red Laser Diode (λ=635 nm, Thorlabs, maximum output power<2 mW)

The data is recorded using two different sensors for a comparative study.

1. CCD sensor (Thorlabs, pixel pitch 4.65 µm)
2. Webcam sensor (Logitech, pixel pitch 2.8 µm)

The same protocol is followed in all the permutation and combinations in these experiments. The performance of the developed microscopes is evaluated using the following parameters.

5.2.1 Resolution of the system

The system's resolution is obtained by using a USAF target (Thorlabs, Positive USAF Test Target, R1DS1P) as an object and holograms are recorded with all the combinations of the aforementioned sources and sensors.

5.2.2 Calibration

Before employing the developed microscope to examine human RBCs, it is calibrated using polystyrene beads of 15μm diameter (Structure Probe, Inc. Supplies, RI n_o= 1.59) immersed in microscope oil (RI n_r = 1.52). To extract the object phase, a reference hologram of the medium surrounding the object (oil) is also recorded. The reference phase obtained from hologram of surrounding medium is deducted from the phase acquired from the hologram recorded with sample in the FOV. The phase subtraction nullifies the phase that remained constant between the exposures (due to aberration etc.) bringing out the phase due to the object alone [65]. The Goldstein branch cut phase unwrapping algorithm is used to convert the wrapped phase distribution into a continuous phase distribution [65]. This continuous phase distribution along with the RI of the polystyrene bead and microscope oil provides the thickness distribution of the object using Eq. (4.17) [64]. The cross-sectional profile is also rendered to show the reconstructed thickness variation which should ideally be close to the value specified by the manufacturer indicating that the technique is suitable for accurate thickness measurement of transparent micro-objects.

5.2.3 Spatial stability

The most important advantage of using LED source is the reduction of parasitic interference fringes which acts as noise. Therefore, it is expected that the spatial stability which depends upon variation in background phase distribution is improved. The spatial stability of the system is quantified by measuring the standard deviation of the phase variation without any object in the FOV. The spatial stability is quantified by the standard deviation of this phase variation. Holograms using both quasi monochromatic LED sources and laser sources are recorded and numerically reconstructed to confirm that spatial stability obtained using an LED source is indeed better than that using a laser source. It is expected that the thickness variation is much higher in the case of a high coherent laser source.

5.2.4 Temporal stability

A time series of holograms is recorded to determine the system's temporal stability. Each hologram was numerically reconstructed and the phase distribution at each time instance is

extracted. The standard deviation of the time variation of phase at each spatial location acts as the measure of fluctuation at that point. The system's temporal stability is measured by the mean value of thickness fluctuations computed at multiple spatial points. Compared to a two-beam setup, which provides a temporal stability of 2-4 nm over the period of several minutes, with vibration isolation [58], the presented common path geometries are expected to provide higher temporal stability without the need of vibration isolation demonstrating that they are more immune to external mechanical noise, due to its self-referencing nature, which inherently reduces the unwanted thickness fluctuations due to mechanical noise

5.2.5 Application in biomedical imaging

After calibrating the system, they are employed for the quantitative phase imaging of Red Blood Cells (RBCs) and extracting some of their physical as well mechanical parameters. On a microscope slide, a thin smear of human blood is prepared, and holograms with and without RBCs in the FOV are recorded. The phase obtained from a hologram containing only blood plasma (reference phase) is deducted from the phase obtained with an object in the FOV, nullifying the constant phase between exposures. This phase is used along with constant average RI of RBCs (1.42) and that of blood plasma (1.34) [278] to reconstruct the thickness profiles of the RBCs.

5.3 Self referencing digital holographic microscopy using Fresnel Biprism

Fresnel Biprism as the self-refencing module with both He-Ne and LED as the illuminating source is explored. A Fresnel Biprism is “a thin double prism placed base to base and have a very small refracting angle (0.5°)”. This is equivalent to a single prism with one of its angles nearly 179°and the other two 0.5° each. It leads to wavefront division interferometric geometry [52,125,279,280]. When a monochromatic light source is placed in front of biprism two coherent virtual source are produced as shown Fig 5.2

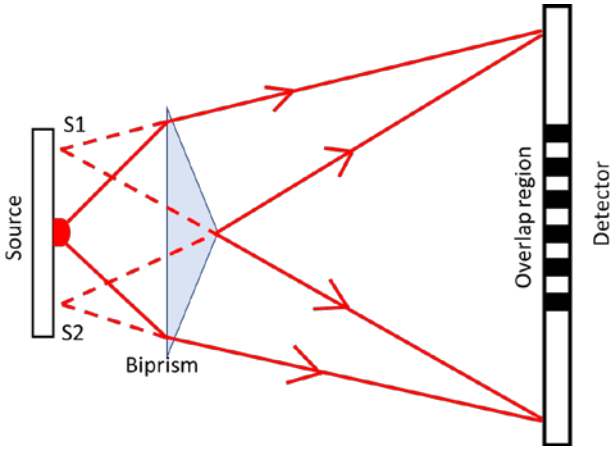

Fig 5.2 A typical Fresnel Biprism based interferometer

Light passes through the biprism, deviates at an angle and interference pattern is produced at opposite side of the source on the screen (which can be a digital array). Consider rays of light falling upon upper prism, if it is seen from the side of the screen, it looks like the rays are expanding from the virtual source S1. Similarly, lower prism, results in a second virtual source S2 [125][52]. To generate interference pattern, two beams of coherent light derived from the same source are required. In the case of bi-prism the two virtual sources S1 and S2 (Fig. 5.2) can be considered to generate the two beams required for generation of the interference pattern. The beams refracted by the two halves of the bi-prisms overlap at the senor plane to produce interference pattern. Interference fringes will appear only where the path difference between the two interfering wavefronts is less than the light source's coherence length, even if the overlap region is large. This region decides the FOV of the microscope, since only regions where interference fringes exist, provide phase information of the object. The angle between the superposing wavefronts, which in turn depends on the angle of the bi-prism, determines the path difference between the two interfering beams. So large apex angle bi-prisms leads to less FOV (especially with low temporally coherent LED sources), as coherence length saturation (coherence length less than path difference) occurs in short span of space. One can argue that using biprisms with smaller apex angle can provide larger FOV. But it is counterintuitive, since lower apex angles leads to smaller overlap regions and hence smaller FOV. Also, the use of smaller apex angles will lead to low density interference fringes, which are very difficult to analyse with Fourier fringe analysis techniques.

5.3.1 Self-referencing digital holographic microscopy using He-Ne and a Fresnel Biprism

The 2D schematic of the table-top version of the developed microscope setup is as shown in Fig 5.3. He-Ne (λ=632 nm, Thorlabs, Maximum output power<2 mW) is employed as the light source. The laser light transilluminates the sample which is imaged using a MO (20X, 0.40NA). A Fresnel biprism (176°, 4cmx5cm) splits the incoming light and recombines it to form hologram on the sensor. These holograms are recorded using a CCD sensor (Thorlabs, 8-bit dynamic range, 4.65 µm pixel pitch) at the rate of 30Hz for 30 sec.

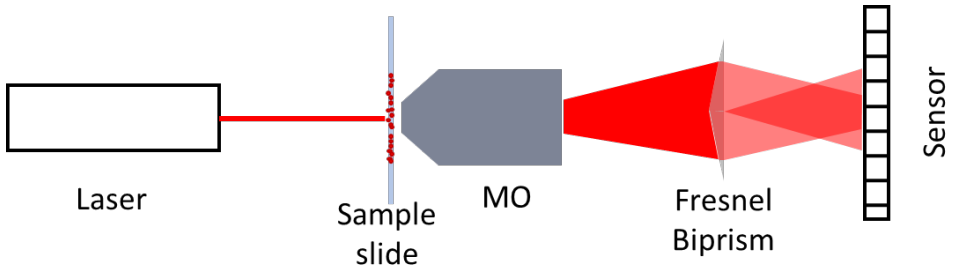

Fig 5.3 2D schematic of the common path self-referencing digital holographic microscope employing He-Ne laser and Fresnel Biprism interferometer

5.3.1.1 Calibration

Fig. 5.4a shows portion of the hologram of 15µm diameter polystyrene microspheres recorded using the devised microscope. The reference phase obtained from the hologram recorded with medium surrounding the microspheres (microscope oil) is subtracted from the object phase obtained from object the hologram shown in Fig 5.4, bringing out the phase only due to the object. The Goldstein branch cut phase unwrapping algorithm is used to convert this wrapped phase distribution into a continuous phase distribution [60] and is represented in Fig 5.4b. The thickness distribution of the object is determined by this continuous phase distribution, as well as the RI values of the polystyrene bead and microscope oil [65] which is shown in Fig 5.4c. The cross-sectional profile of thickness shown in Fig 5.4 d shows that the reconstructed thickness variation is almost close to the manufacturer specified value indicating that the technique is suitable for accurate thickness measurement of transparent micro-objects.

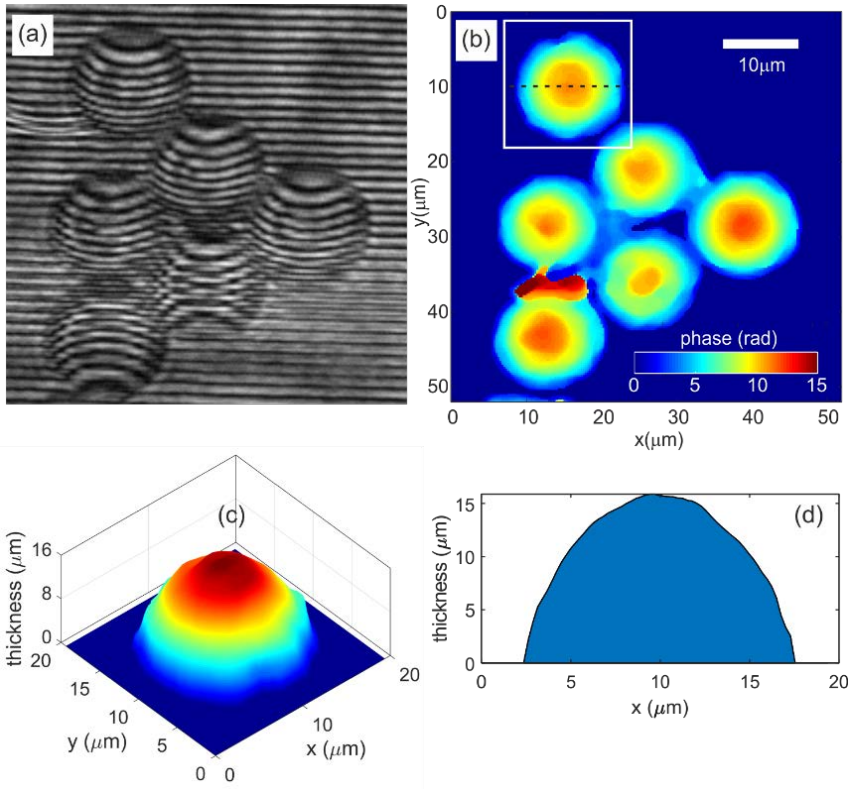

Fig 5.4 (a) recorded hologram of polystyrene beads (b) continuous phase distribution obtained after unwrapping (c) thickness distribution of the Polystyrene beads (d) cross-sectional thickness of the polystyrene microsphere. He-Ne laser source is used to illuminate the sample.

5.3.1.2 Imaging Red blood cells

A thin smear of human blood prepared on a microscope glass slide is used as the object and holograms of this sample are recorded (at the rate of 30Hz for 30s) with and without RBCs in the FOV. The phase obtained with the object in the FOV is subtracted from the reference phase obtained from a hologram containing only blood plasma. Fig 5.5a shows the hologram of the human RBCs recorded with red He-Ne source. Fig 5.5b represents the quantitative phase images retrieved after phase subtraction. This phase image along with constant average RI of RBCs (1.42) and that of blood plasma (1.34) [278] are used to reconstruct the thickness profiles of the RBCs shown in Fig 5.5c. Fig 5.5 (d) shows the cross-sectional thickness profile of the RBC and the figure shows its doughnut profile

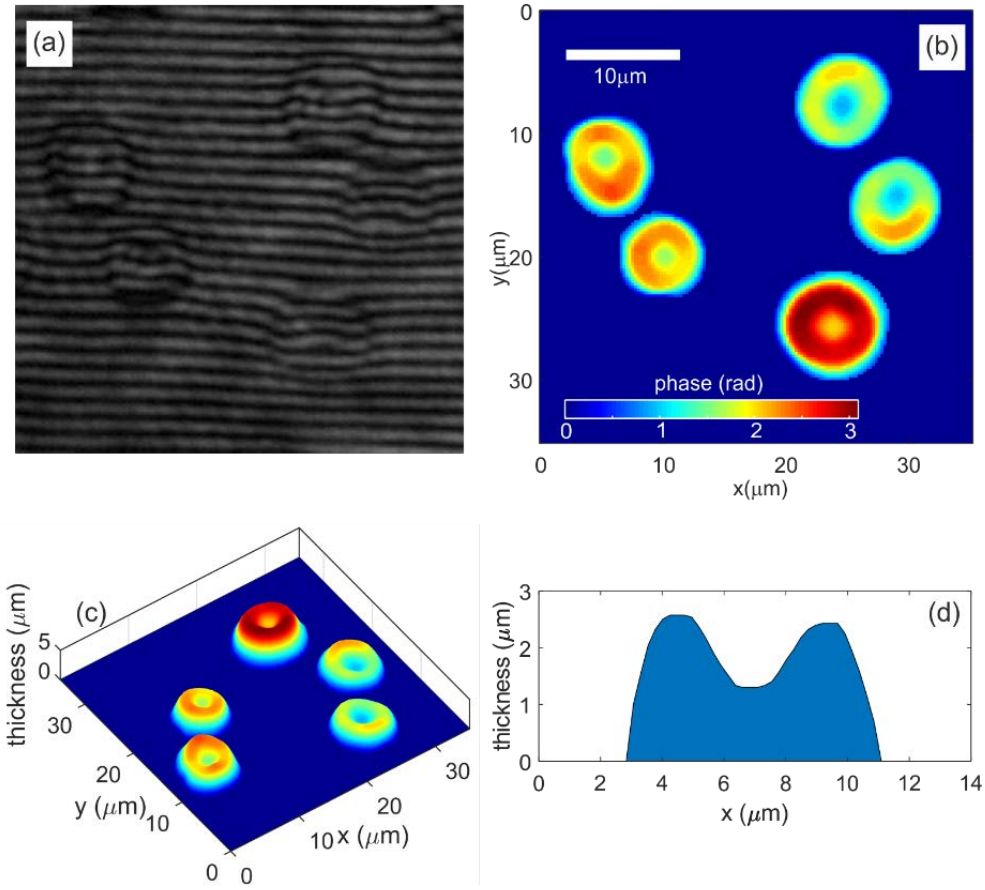

Fig 5.5 (a) recorded holograms of the RBCs (b) continuous phase distribution after unwrapping (c) thickness distribution of the RBCs (d) line profile of the thickness distribution. He-Ne laser source is used to illuminate the sample.

5.3.2 Self-referencing digital holographic microscopy using LED and a pair of Fresnel Biprism for hologram multiplexing

Use of LED source reduces the region in which high contrast fringes results, due to lower temporal coherence. To increase the FOV, hologram multiplexing using multiple parallel biprisms, which will lead to simultaneous generation of multiple regions of interference fringes is employed. The 3D schematic of the tabletop version of the hologram multiplexing microscope setup is shown in Fig 5.6. An LED (Lumilux, λ=627nm, maximum power output of 2W, Δλ=20nm) with emitting area 1mm^2 is employed as a source of light. This size of the source is reduced with the help of 10x MO in order to increase the spatial coherence area of the source. The de-magnified source illuminates the sample which is imaged using a 20X, 0.40NA MO. A pair of Fresnel biprism (176°) with the same specification is placed on the path of the object beam. This wavefront division module splits the incoming light and recombines it to form multiple holograms on the same sensor array. These holograms are recorded using a CCD sensor (Thorlabs, 8-bit dynamic range, 4.65 μm pixel pitch) at the rate of 10Hz for 30 seconds.

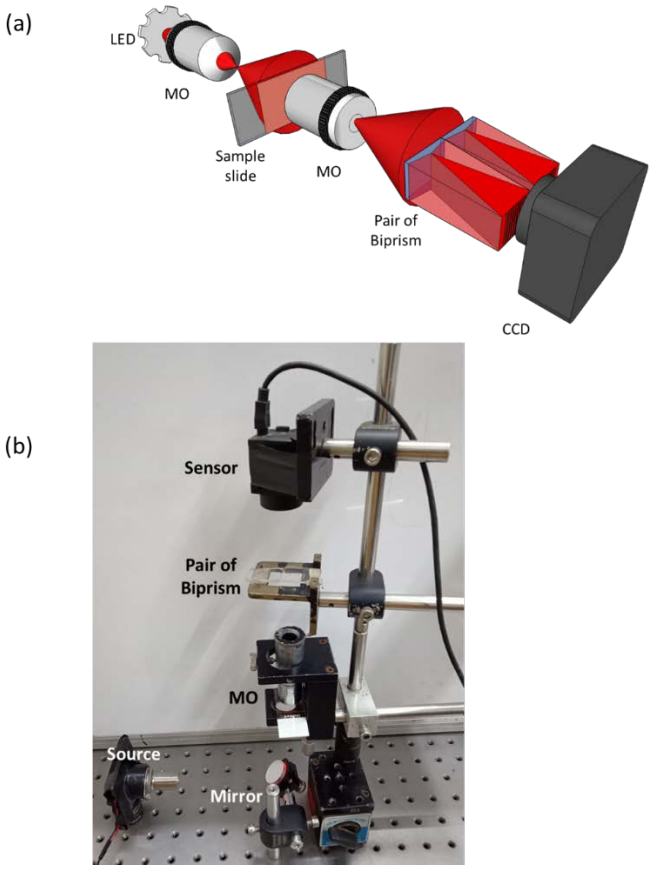

Fig 5.6 (a) shows the 3D schematic of the common path self-referencing digital holographic interference microscope employing a pair of Fresnel biprisms and LED source (b) Tabletop setup in the laboratory (VideoV1 shows the working of the tabletop setup)

5.3.2.1 Spatial stability

It is expected that the spatial stability, which depends upon variation in background phase distribution to be improved due to the use of a low temporally coherent LED source, leading to the smoother background and lower speckle noise and noise due to parasitic interference patterns. To find the improvement in Signal to Noise Ratio (SNR) in using LED source compared to laser source, holograms using both Laser and LED sources are recorded. Fig 5.7a and c shows the 3D rendering of the reconstructed optical path length distribution without any object in the FOV with a laser source and the LED source, respectively. From these figures, it can be noted that the optical path length variation is higher in the case of laser source. From the histograms (Fig 5.7c and d) of the spatial variation of optical path length, it can also be seen that the SNR with LED source is better than two times that using laser source, which will lead to improved thickness measurement using LED sources.

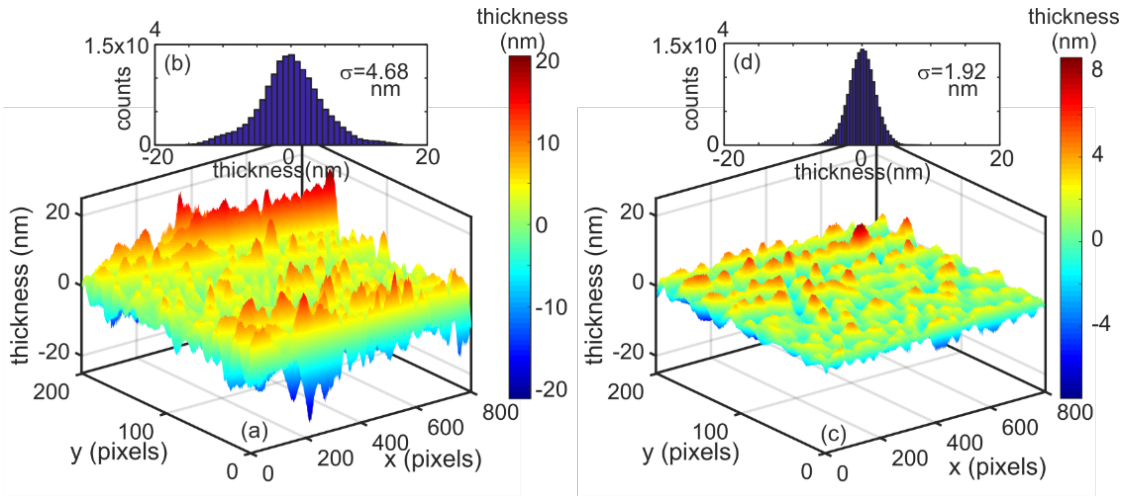

Fig 5.7 Spatial stability (a) spatially varying optical path length using laser source (b) histogram of the spatial thickness variation along with the standard computed standard deviation value for laser source. (c) spatially varying thickness using LED source (d) histogram of the spatial thickness along with the standard computed standard deviation value for LED source. σ in the histogram represents the standard deviation of the optical path length

5.3.2.2 Temporal Stability

The temporal stability of the system is determined by recording a time series of holograms (10Hz, 30s). The presented common path setup provides higher temporal stability, since the object and the reference beams travel along the same path and interacts with the same set of optical components. The spatial mean of standard deviation of the time varying optical path length variation is the measure of the temporal stability of the device [64]. The measured temporal stability, without dedicated vibration isolation, of the describe technique over 15 seconds is 0.91 nm, demonstrating that it is more immune to external mechanical noise as shown in Fig 5.8.

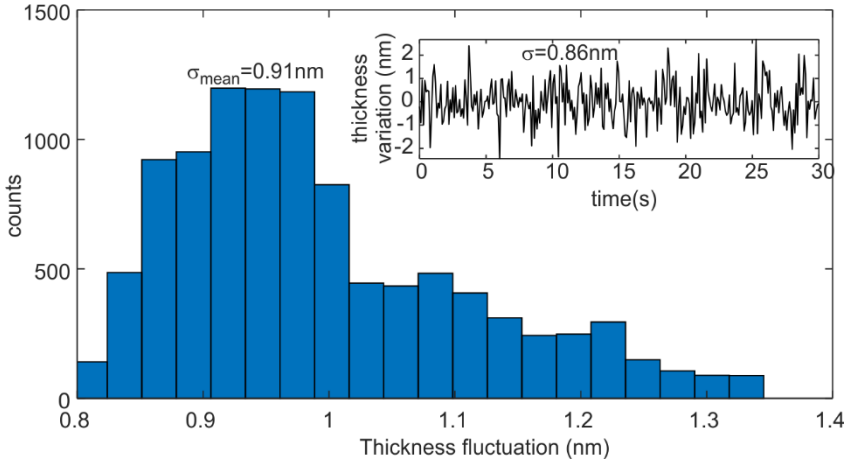

Fig 5.8 Temporal stability of the system. Histogram represents the measured counts for thickness fluctuation at each spatial point (standard deviation of time varying thickness). The mean of these values represents the temporal stability of the microscope. Inset shows the time varying thickness at one spatial point..

5.3.2.3 Calibration

Calibration of the system is carried out using 15μm diameter polystyrene microspheres. The wrapped phase difference between the object hologram (Fig. 5.9a) and reference hologram is converted into continuous phase distribution [60] shown in Fig 5.9b. This continuous phase distribution along with the RI values of the polystyrene bead and microscope oil provides the thickness distribution of the object [65] as shown in Fig 5.9c. The cross-sectional profile shown in Fig 5.9d shows closeness of the reconstructed thickness variation to the manufacturer specified value.

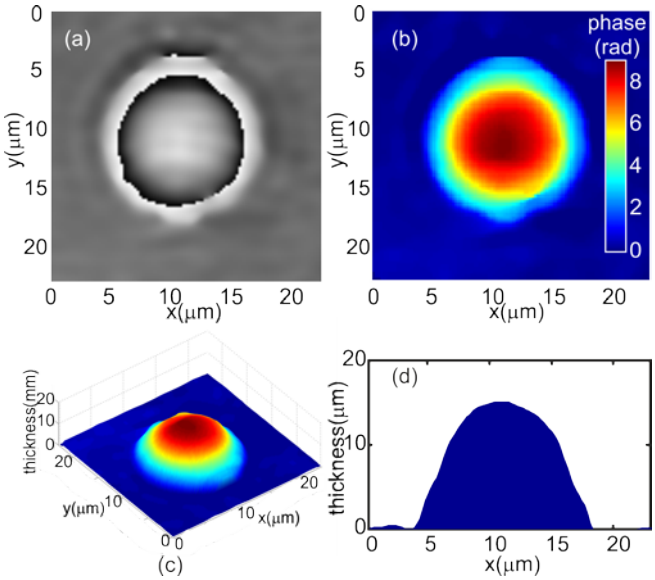

Fig 5.9 Reconstructed wrapped phase distribution of polystyrene beads (b)continuous phase distribution obtained after phase unwrapping (c) thickness profile (d) line profile of the thickness distribution. LED source (λ=627nm) is used to illuminate the sample.

5.3.2.4 Imaging Red blood cells

As in the case for Laser illumination, a thin smear of human blood is prepared on a microsope glass slide and used as the object. Holograms of this sample are recorded at the rate of 10Hz for 30s with and without RBCs in the FOV. Fig 5.10a shows the hologram of the human erythrocytes recorded with red LED source. Quantitative phase image obtained after phase deduction is shown in Fig 5.10b. Thickness distribution of RBC after plugging in the constant average RI values for the RBC and blood plasma in Eq. 4.16 is shown in Fig 5.10c. Cross sectional thickness profile of RBC is shown in Fig. 5.10d.

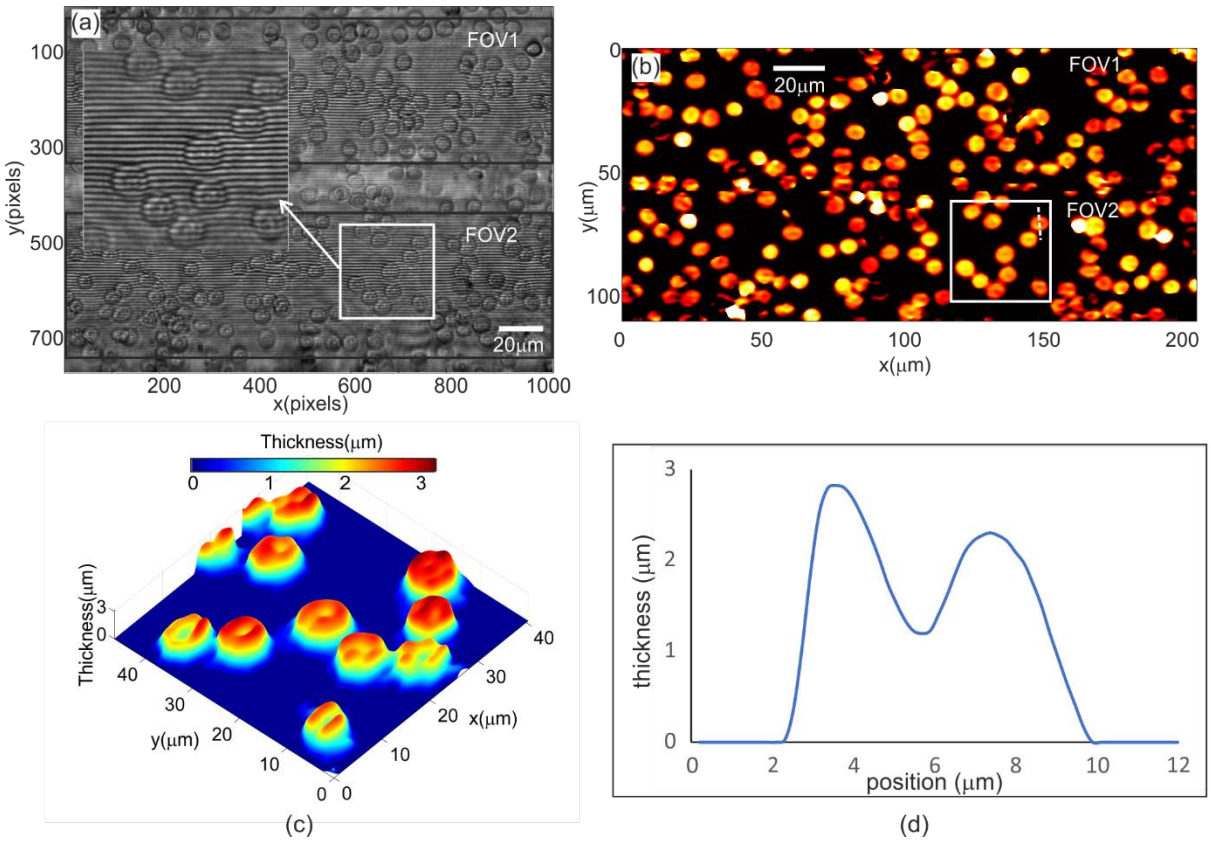

Fig 5.10 Quantitative phase imaging of human erythrocytes using LED source and multiplexed holograms (a) recorded multiplexed hologram (b) quantitative phase imaging corresponding to the two fields of views marked in Fig 5.10a(c) 3D rendering of thickness distribution of RBCs inside the area of interest marked by white rectangle (d) cross sectional thickness profile of the RBC along the dashed line marked in Fig 5.10b

The advantage of the technique is that the path length of the object and reference beams are automatically matched for all the multiplexed holograms. This makes the method ideal to be used along with short wavelengths, where the coherence length is further restricted. The use of short wavelengths also leads to higher lateral as well as axial resolution. In order to improve both the lateral and axial resolution in the system, the use of exotic UV wavelength (Luxeon UV LED, λ=385 nm, maximum power output of 425mW, $\Delta\lambda$=9nm, coherence length~7.2mm) is also explored. Fig 5.11a shows the portion of the self-referencing hologram of RBCs recorded with UV LED as the illuminating source. Fig 5.11bshows the optical thickness distribution of RBCs obtained after numerical processing of the recorded hologram and phase subtraction.

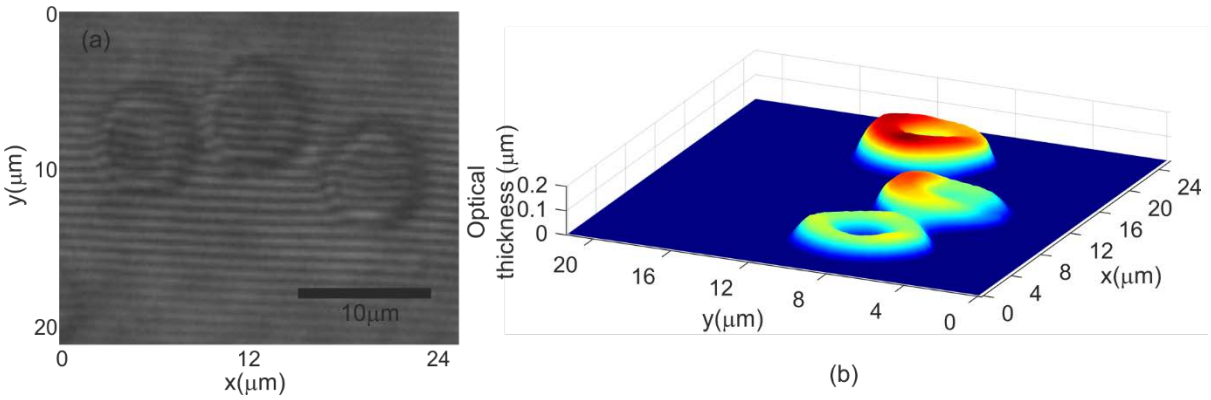

Fig 5.11 Quantitative phase imaging of human erythrocytes using UV LED and multiplexed holograms (a) Portion of the recorded multiplexed hologram (b) 3D rendering of thickness distribution of RBCs

5.3.2.5 Improvement in lateral resolution

The improvement in lateral resolution of the digital holographic microscope at UV wavelength is tested by recording holograms of USAF resolution targets. Fig 5.12a and Fig 5.12b shows the portion of the holograms of the USAF resolution target (Group 7, Element 6, Linewidth 2.2mm) recorded with LEDs working at 627nm and 385nm respectively. Fig 5.12c and shows the reconstructed intensity profile obtained from the numerically processed holograms. Fig 5.12e shows the line profile of the intensity variation along the solid lines in Fig 5.12c and d indicating improvement in lateral resolution with the UV illuminating source.

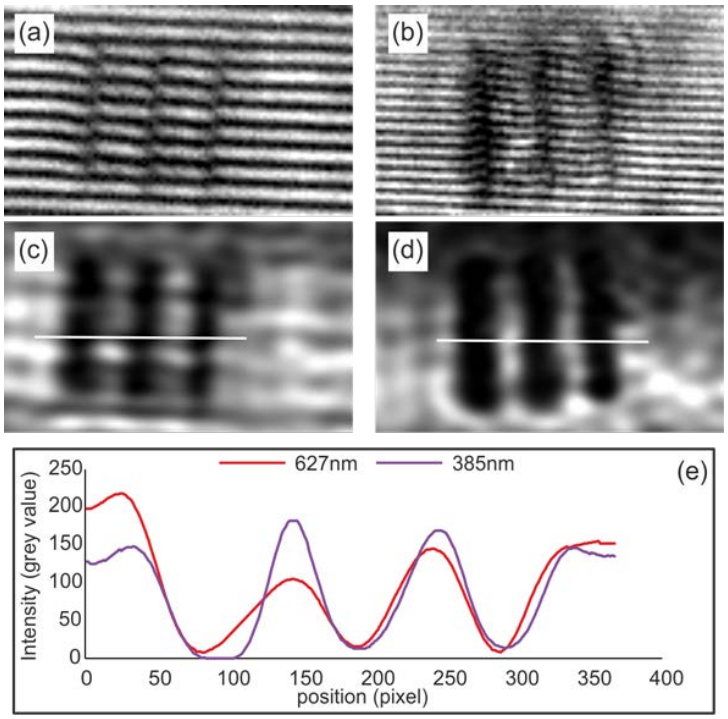

Fig 5.12 Improvement in lateral resolution at shorter wavelengths (a) and (b) portions of recorded hologram showing line structure of Group 7 element 6 of the resolution target using 627nm and 385nm LED sources respectively. (c) and (d) represent the reconstructed intensity patterns for 627nm and 385nm LED sources (e) line profile of the intensity variation

The recent boost in the field of 3D printing has facilitated the fabrication of printed devices which are portable and provide sturdy framework. The concept of parallel biprism to improve the FOV has been incorporated into a 3D printed module allowing it to work as a stand-alone device which can be deployed to various remote parts where availability of expensive diagnostic tools is scarce. Fig 5.13a shows the 3D printed module of the microscope. Fig 5.13a shows the labelled parts,5.13b shows the dimensions of the fabricated device and module Fig. 5.13c demonstrates working of the device.

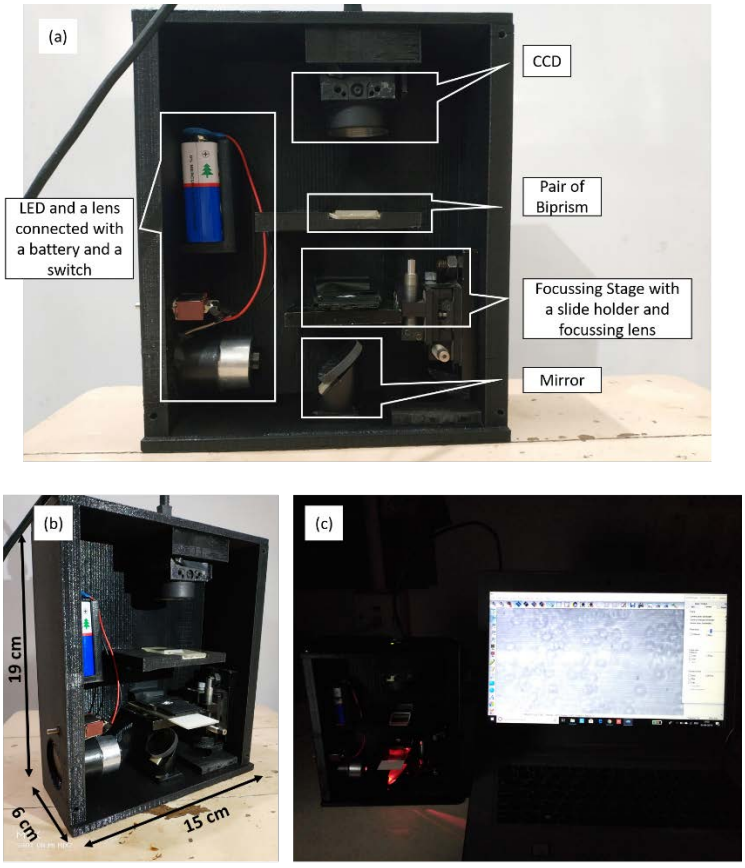

Fig 5.13 3D printed Fresnel biprism device with optical and imaging components (b) dimensions of the setup (c) device in working mode

5.4 Self-referencing digital holographic interference microscopy using Lloyd's mirror interferometer with increased field of view

The next investigates microscope geometry employed the Lloyd's mirror interferometer for generating holograms and examining the biological samples. This geometry was first described by Humphrey Lloyd in 1834. The Lloyd's mirror geometry works on the principle of wavefront division [80,281,282]. It consists of either a flat piece of dielectric or a mirror from which portion of the primary wavefront is folded such that it interferes with the unfolded portion of

the same wavefront which is coming directly from the primary wavefront as shown in Fig 5.14. This geometry is considered as a common path self-referencing geometry in which both the beams travel the same path. The main advantage of this geometry is that it is relatively compact and, stable compared to the two beam geometries and enables us to have a variable fringe density without any flux loss so as to obtain high contrast interference fringes.

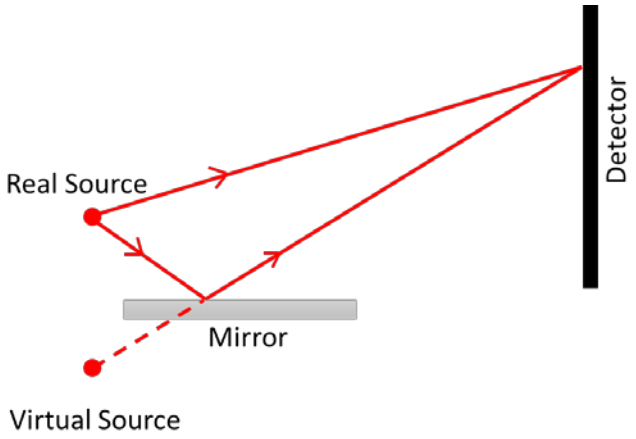

Fig 5.14 A typical Lloyd's mirror interferometer

5.4.1 Compact, low cost, large field-of-view Lloyds mirror digital holographic microscope using laser diode module

Fig 5.15 a and b shows the schematic of the developed Lloyds mirror based digital holographic microscope that uses an off the shelf laser diode module (unpolarized, $\lambda = 635$ nm, power < 2 mW) as the source. The laser beam illuminates sample under examination. Sample is prepared in such a way that only half of the source beam illuminates the it and the other half passes through unperturbed (Fig 5.15 b). The beam then passes through the magnifying lens, which is an achromat of focal length 8.3 mm and clear aperture of 7 mm, extracted from a commercial grade MO lens. The numerical aperture of the lens is 0.4. The portion of the laser beam passing through the object is modulated by object information and the rest of the laser beam remains unmodulated as shown in Fig 5.15b. The modulated and unmodulated portions of the illuminating beam, pass through the magnifying lens. The modulated portion of the laser beam (object beam) directly reaches the hologram recording sensor, which is a webcam (Logitech, C370, RGB, 1.3MP, 2.8 μm pixel pitch), with its imaging lens removed. The unmodulated portion (reference beam) is reflected on to the recording sensor using a mirror (2.5 cm × 2.5 cm). The object and the reference beams interfere at the webcam leading to generation of holograms (at the hologram plane, the lens provides a magnification of 30x). The webcam is

placed in such a position where the contribution from the interference is dominant compared to the diffraction pattern arising due to the edge of the mirror.

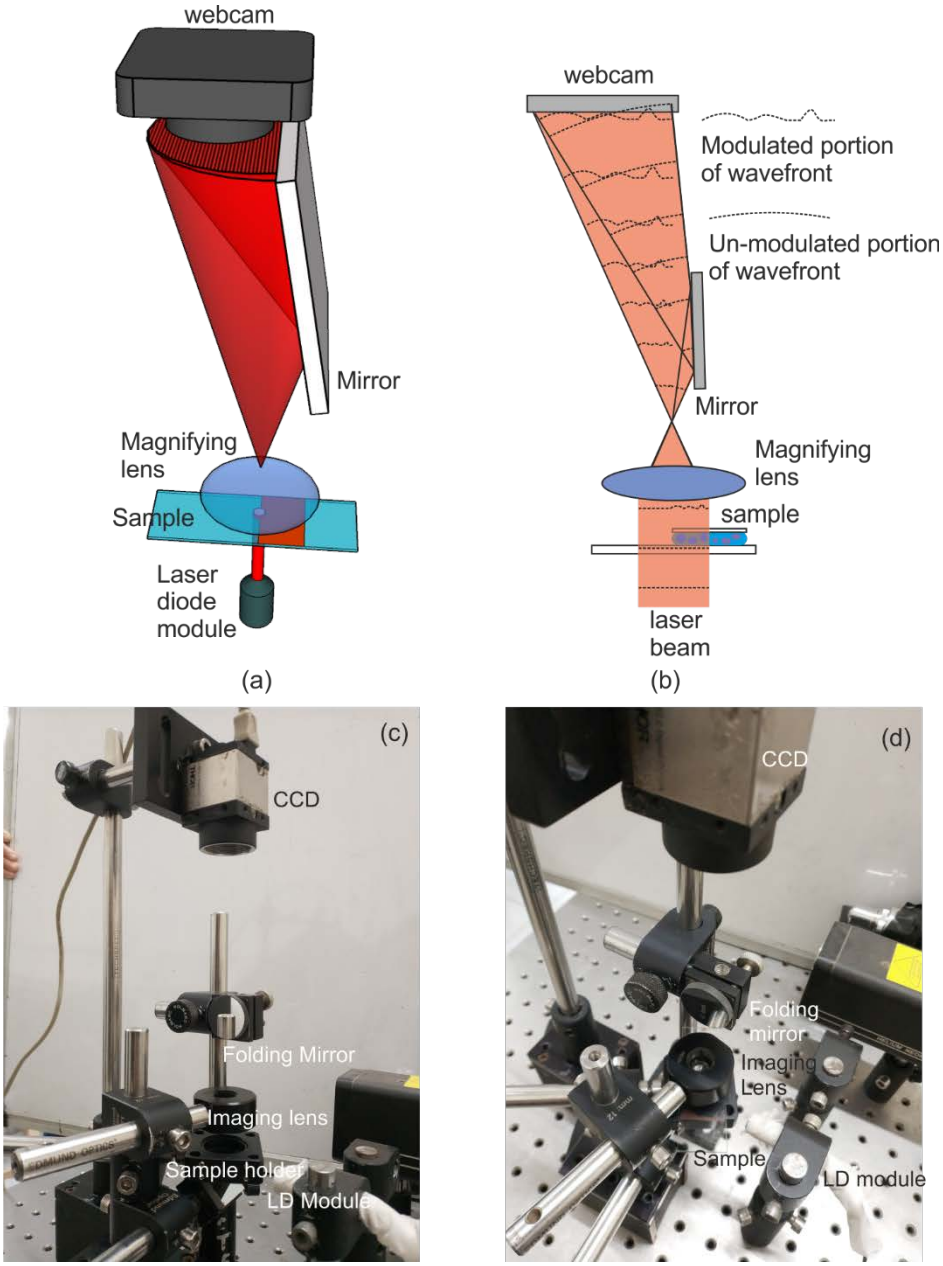

Fig 5.15 (a) Large field of view wavefront division digital holographic interference microscope employing Lloyd's mirror configuration. (b) Interference of modulated and un-modulated portion of the laser beam leading to creation of holograms (c) and (d) table top version of the microscope in the laboratory

It should be noted that the magnifying lens is fixed and no mechanical movement is used for focusing the sample. During the construction of the microscope, the sensor is positioned at the image plane of the magnifying lens and a stage having two platforms with a separation equal to the distance between the sample and the magnifying lens was 3D printed to hold the sample and the magnifying lens. This ensured that the introduction of the sample, did not shift the best

focus plane. The defocusing due to change in the position of the sample (from the position at which best focus results) is removed by the means of numerical focusing at the time of hologram reconstruction. One of the advantages of this configuration is that the mirror can be tilted to achieve the desired fringe density, which is an important parameter in the numerical processing of the holograms [80,124]. This aspect is difficult to achieve in other common self-referencing methods. Also, since the object and reference beams are derived from the same wavefront, it leads to automatic matching of the beam intensities resulting in high contrast fringes (holograms). The use of 3D printed platform for holding the sample, ensures compactness and higher temporal stability which may not be possible using a translation stage since it is bulky and may introduce additional mechanical noise.

The holograms in this proposed geometry are obtained using the principle of wavefront division wherein "two coherent sources are generated by dividing the wavefront originating from a common source by employing a mirror" as shown in Fig 5.15. Here, portion of the beam directly falling on the sensor contains object information and beam that is reflected by the wavefront division mirror acts as a reference creating a self-referencing geometry.

Fig 5.16 shows device fabricated by 3D printing the support structure and then integrating the optical components and imaging device. The dimensions of the fabricated device were 18 cm × 15 cm× 5.5 cm. The device weighed less than 600 g.

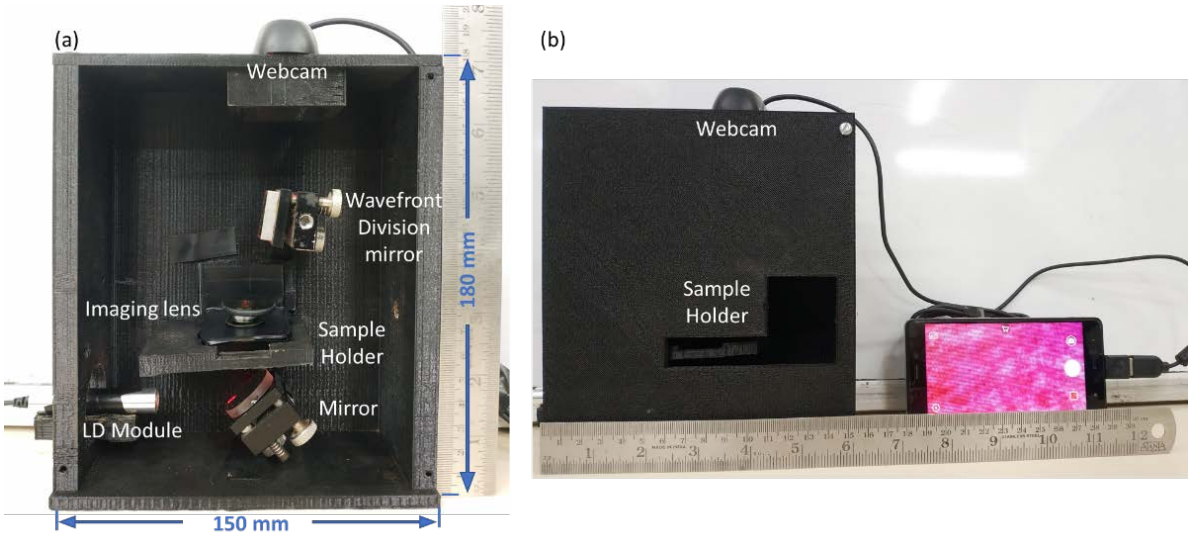

Fig 5.16 (a) Dimensions of the field portable 3D printed microscope (b) 3D printed module attached with a mobile phone through OTG cable (Video 2 shows the working of the 3D printed device employing Lloyd's mirror)

5.4.1.1 Temporal stability

Temporal stability was quantified by recording a series of holograms for 30s at the rate of 30Hz using the webcam. The mean (over the field of view) of the standard deviation of time varying phase provides the temporal phase stability of the setup. The path length variation over a period of 15s was measured to be 0.68nm, which is comparable with the other reported self-referencing geometries [22,54,58,65,69,80,126,279]. Fig 5.17 shows the histogram that represents the measured counts for thickness fluctuation at each spatial point (standard deviation of time varying thickness). The mean of these values represents the temporal stability of the microscope. Inset shows the time varying thickness at a spatial point in the FOV.

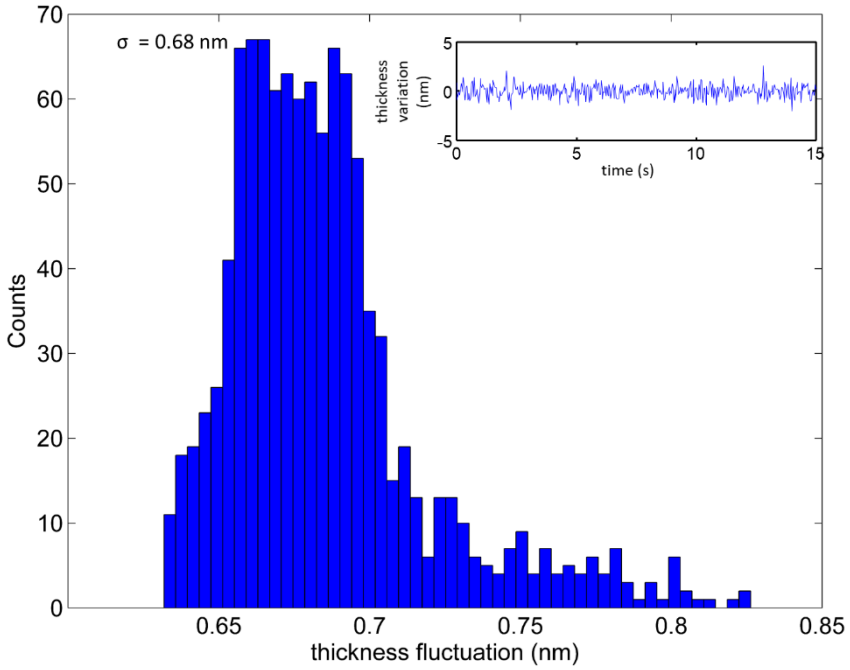

Fig 5.17 Temporal stability of the system. Histogram represents the measured counts for thickness fluctuation at each spatial point (standard deviation of time varying thickness). The mean of these values represents the temporal stability of the microscope. Inset shows the time varying thickness at a spatial point in the field of view.

5.4.1.2 Field of view improvement

The designed microscope has larger usable FOV compared to the configuration which was suggested previously [9]. This is due to the fact that the sample is introduced in only one half of illuminating laser beam, leading to generation of completely un-modulated (object information free) reference beam. This is because of the use of large aperture lens for imaging, which allows easy introduction of the sample in only a pre-defined area of the illuminating laser beam. In the work reported earlier [80], the sample was introduced in the whole of the illuminating laser beam leading to overlapping of the sample information from the direct beam

and the beam folded on to the sensor by the mirror leading to reduced usable FOV. Moreover, since a large portion of the illuminating beam should be clean enough to act as the reference, only sparse object distributions could be imaged. Fig 5.18a shows the reconstructed phase distribution in the case where the object is introduced in the path of the entire laser beam compared to the phase distribution obtained using the described geometry shown in Fig 5.18b. It can be clearly seen that the present setup provides better phase reconstructions especially for dense object distribution, along with large usable FOV (almost double that of the conventional self-referencing geometry).

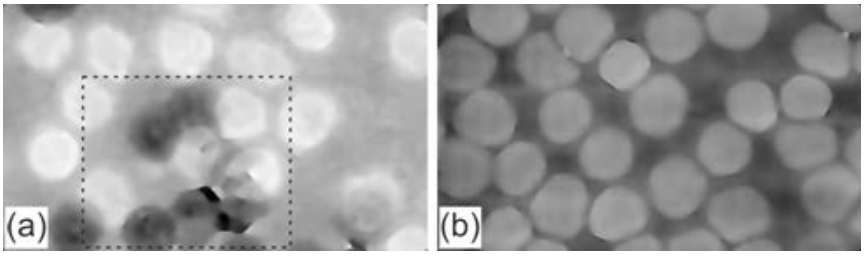

Fig 5.18 Reconstructed phase distribution in the case where (a) the object is introduced in the path of the entire laser beam and (b) the object was introduced in a portion on the illuminating laser beam. The overlap of images from the direct beam and the beam folded on to the sensor by the mirror can be seen (inside the dashed rectangle).

5.4.1.3 Calibration

As in the previously described setups, calibration of the microscope was carried out using 15μm diameter polystyrene microspheres immersed in microscope oil as sample. Fig 5.19a shows the wrapped phase distribution of the recorded hologram of the polystyrene beads. Phase reconstructed from the reference hologram is subtracted from the phase reconstructed from the object hologram to yield the object phase distribution. This wrapped phase distribution was then converted into continuous phase distribution which is shown in Fig 5.19b. The spatial variation in sample thickness is shown in Fig 5.19c and the cross-sectional profile of the thickness distribution is shown Fig 5.19d.

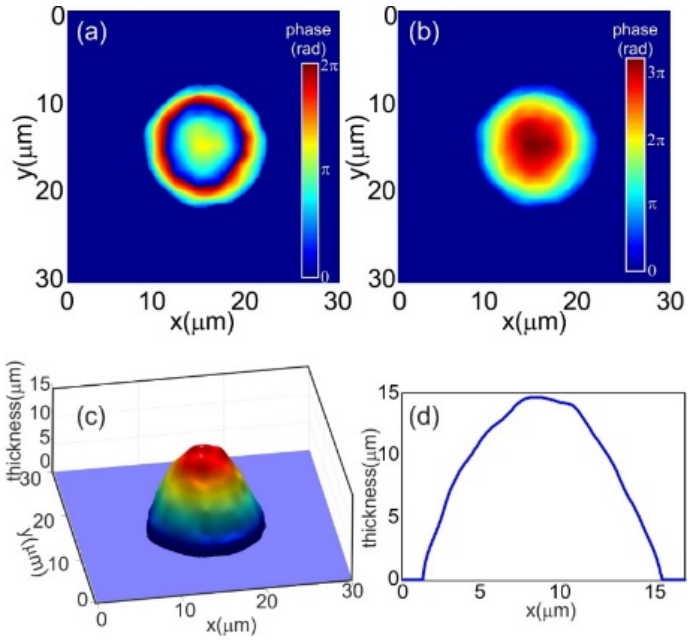

Fig 5.19 Microscope calibration using 15μm diameter polystyrene microspheres. (a) Wrapped phase distribution obtained after phase subtraction (b) Continuous phase distribution obtained after phase unwrapping. (c) Thickness distribution of the microsphere. (d) Cross-sectional profile of the thickness distribution.

5.4.1.4 Imaging Red blood cells

In the next set of experiment, thin smears of blood samples were investigated and the technique was used to extract RBC parameters, based on its reconstructed morphology (thickness distribution). The holograms were recorded at 30Hz for 30 seconds. Hologram of the blood cells is shown in Fig 5.20 (a). For each set of object holograms, a reference hologram which only had blood plasma in the FOV was recorded. Fig 5.20 (b) shows the continuous phase distribution across the whole FOV in the case of RBCs after phase unwrapping. The cell thickness distribution is shown in Fig 5.20 (c).

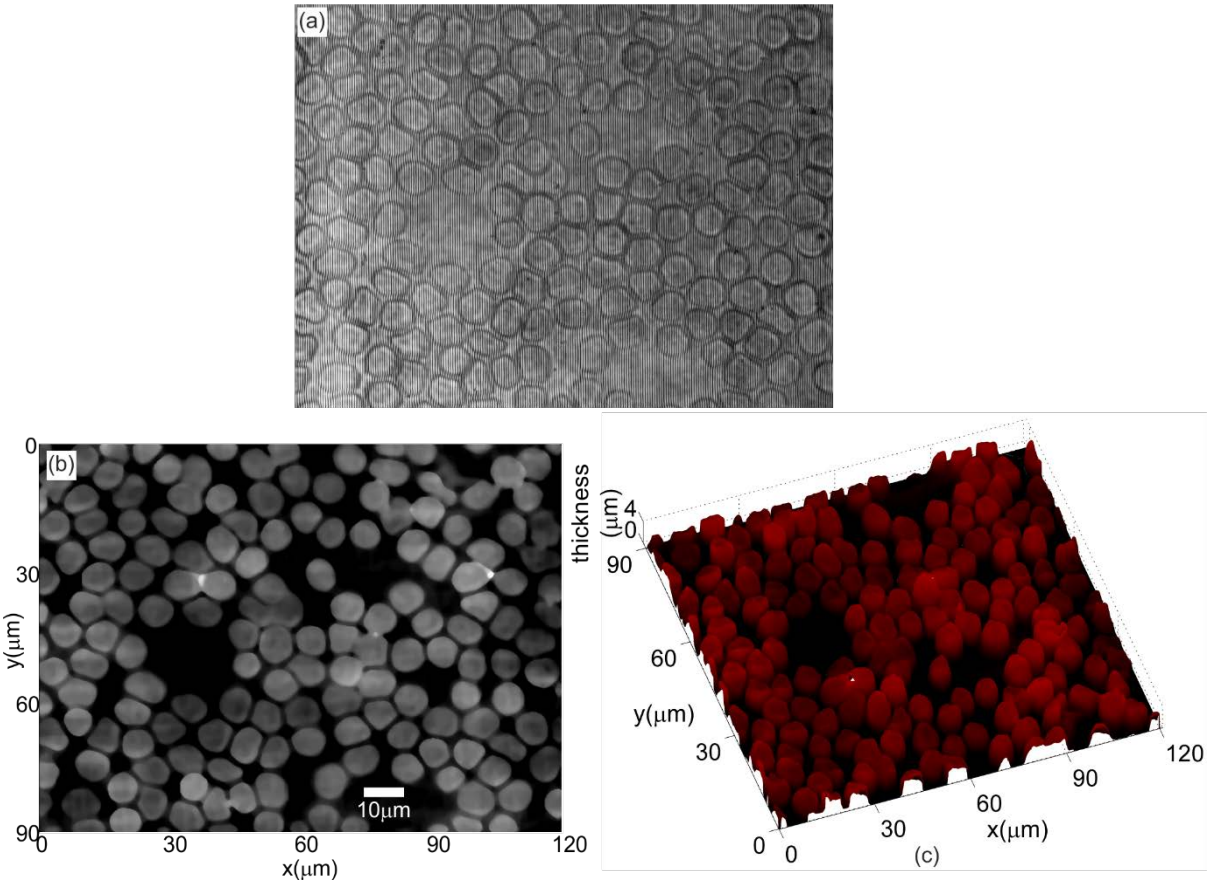

Fig 5.20 Quantitative phase imaging of red blood cell distributions. (a) Recorded hologram of a dense distribution red blood cell (b) Continuous phase distribution obtained after phase subtraction. (c) Thickness distribution computed from the continuous phase distribution.

5.4.2 Digital holographic microscopy using LED and Lloyd's mirror

Lloyds mirror geometry leads to automatic matching of optical path lengths of the object and reference beams at the detector plane, making it ideal for implementation along with LED sources. However, as the coherence length of quasi-monochromatic LEDs are low (few micrometres), for large field of, hologram multiplexing is necessary. The use of LED and hologram multiplexing in Lloyd's mirror Digital Holographic Microscopy was investigated (Fig. 5.21). An LED (λ=627 nm, Luxeon star, max output power=2W, emitting area 1 mm^2) is used to illuminate the sample. As in the case with Fresnel biprism, size of the source is reduced with the help of a 10x MO lens to increase the spatial coherence area at the sample plane. Light after passing through the expanding lens (MO) illuminates the sample and then passes through an imaging MO (20x, 0.40NA). Two mirrors of dimension 2.5cmx2.5cm are used to fold two different regions of the object beam onto itself and the holograms are recorded using a CCD sensor (Thorlabs, 8-bit dynamic range, 4.65 μm pixel pitch). Unlike the Laser source, LEDs have a lower temporal coherence due to which the interference fringes are formed over small region of the sensor. Hence, two mirrors of the same specifications kept parallel to each other

are used to fold the beam onto itself to generate two sets of fringe pattern which would eventually increase the usable FOV. Fig 5.21a shows the 3D schematic of the common path self-referencing digital holographic interference microscope employing Lloyd's mirror interferometer and LED. Fig 5.21b shows the tabletop setup in the laboratory.

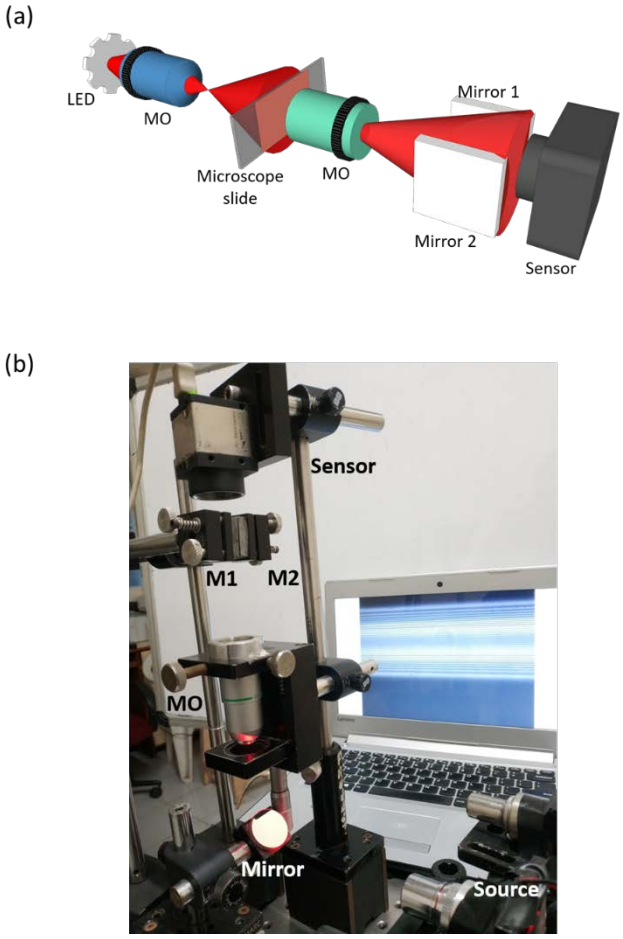

Fig 5.21 shows the 3D schematic of the common path self-referencing digital holographic interference microscope employing Lloyd's mirror interferometer and LED (b) shows the table top setup in the laboratory

5.4.2.1 Calibration

15µm polystyrene microspheres immersed in microscope oil is used for calibration of the microscope. Fig. 5.22a shows portion of the recorded object hologram as Fig 5.22b is the continuous object phase distribution obtained after phase subtraction. Use of the RI of the microsphere and the microscope oil yield the sample thickness distribution shown in Fig. 5.22c and 5.22d.

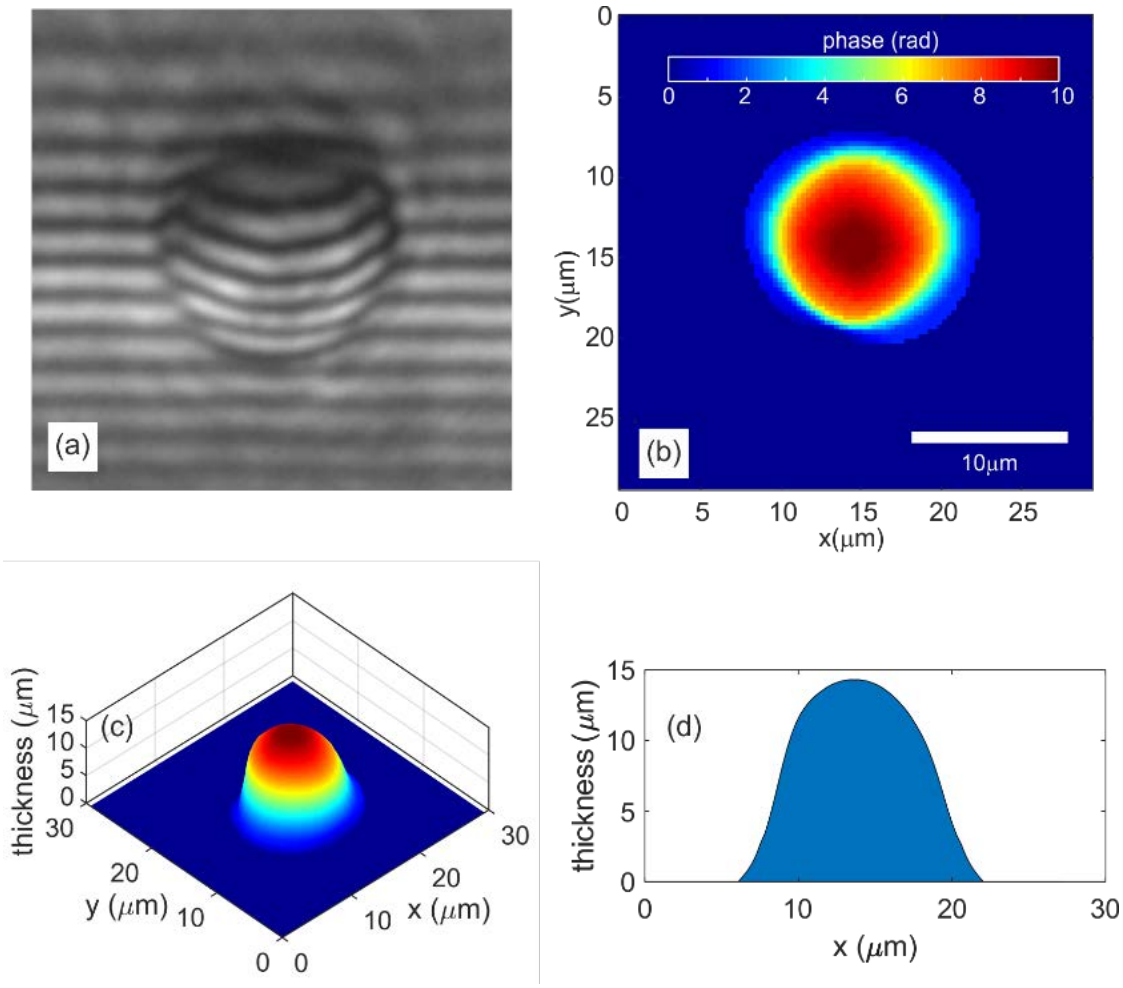

Fig 5.22 (a) recorded hologram of polystyrene beads (b) continuous phase distribution obtained after unwrapping (c) thickness distribution of the Polystyrene beads (d) line profile of the polystyrene bead

5.4.2.2 Imaging Red blood cells

Thin smears of blood samples were investigated for reconstructing thickness distribution of blood cells. Fig. 5.23a shows portion of the recorded object hologram in the case of blood cells. This hologram is numerically processed to extract the phase distribution shown in Fig. 5.23b. The cell thickness distribution obtained after using RI for the red blood cells and blood plasma is shown in Fig 5.23c and Fig 5.23d.

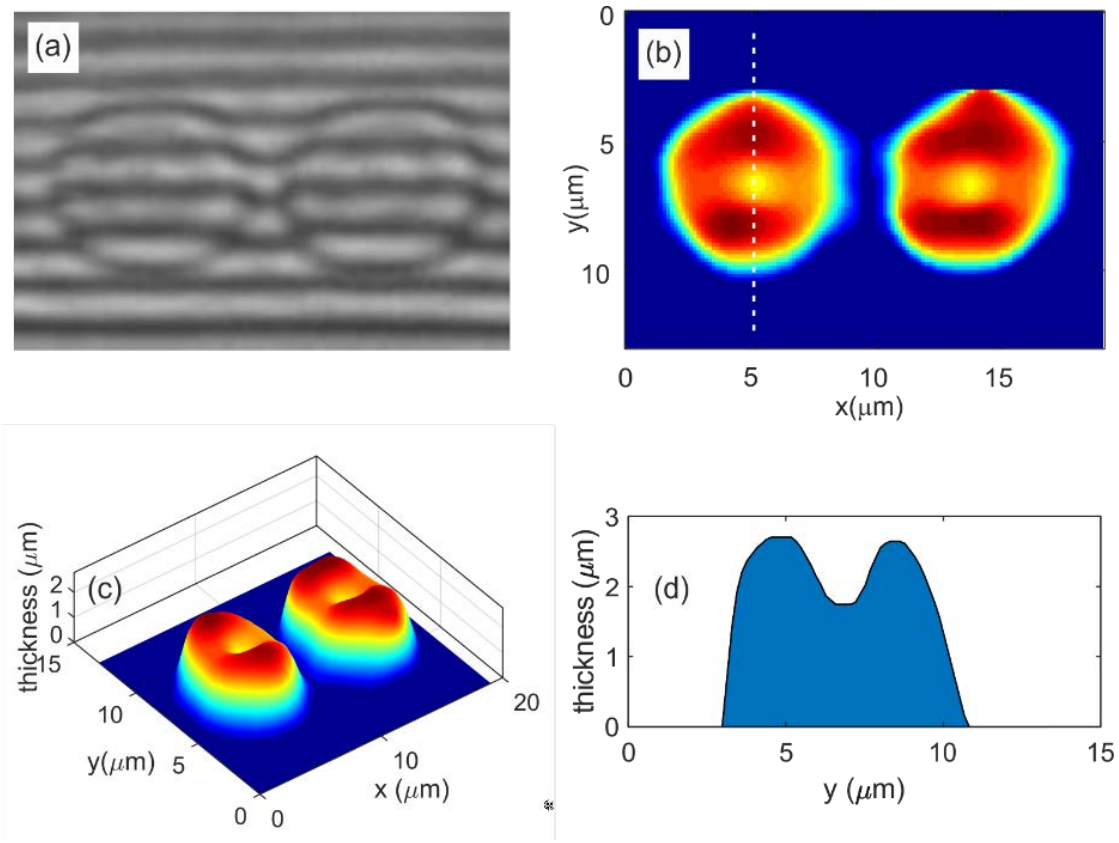

Fig 5.23 Quantitative phase imaging of human erythrocytes using LED source and Lloyd's mirror (a) recorded hologram (b) continuous phase distribution of the recorded RBCs (a) (c) 3D rendering of thickness distribution of RBCs inside the area of interest marked by white rectangle (d) cross sectional thickness profile of the RBC along the dashed line marked in Fig 5.23 (b)

5.5 Digital holographic microscopy using Sagnac interferometer

Sagnac interferometer employs a ring/cyclic geometry. It was first demonstrated by French physicist Georges Sagnac in the year 1913. He showed that "if a beam of light is split and sent to traverse in two opposite directions in a closed loop with mirrors on its perimeters, it will exhibit interference effect" [283]. The Sagnac interferometer is based on the principle of amplitude division in which two beams come across the same set of optical components while travellling in different direction and are later folded onto one another by reflection off the mirrors to obtain the self-referencing configuration [64,284–287]. A typical Sagnac interferometer is shown in Fig 5.24 in which the ring geometry is quite apparent. A slight variation in the phase is introduced in one of the beams which produces a fringe pattern whose spatial frequency can be changed by changing the angle of one of the mirrors. Since it is a self-referencing geometry, employing a low coherent source such as LED to generate interference fringes using this interferometer becomes easy as the path length between both the beams automatically matches.

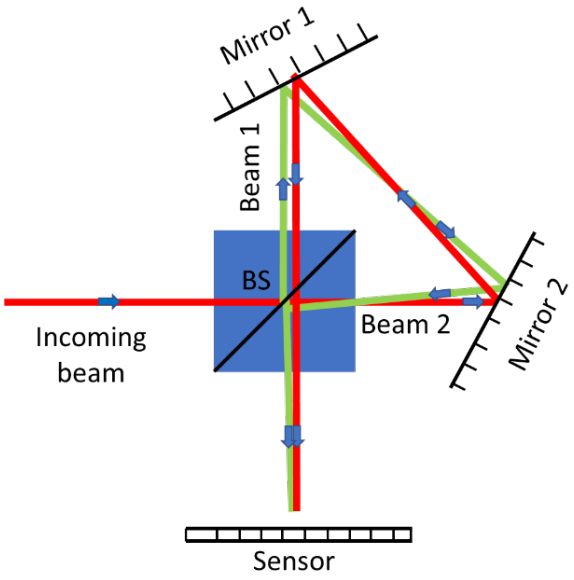

Fig 5.24 A typical Sagnac interferometer

5.5.1 Digital holographic microscopy using Sagnac interferometer and He-Ne laser

Sagnac configuration provides a self-refencing geometry ideal for digital holographic microscopy. Initially, it is investigated for development of a self-referencing digital holographic microscope using He-Ne laser (long temporal coherence) as shown in Fig. 5.25. Output from the laser source illuminates the sample slide and a MO (20x, NA=0.65) is used to image and magnify the object information. This object beam is split using a beam splitter of dimensions 2.5cmx2.5cmx2.5cm. Reflected and transmitted beams from the beam splitter are reflected using front coated mirrors of dimensions 2.5cmx2.5cm. Both the beams after travelling in opposite directions and encountering the same set of optical elements exit the interferometer and recombine to generate interference fringes. The above-described setup creates an off-axis geometry and the interference pattern is recorded with a CCD sensor (Thorlabs, 8-bit dynamic range, 4.65 µm pixel pitch).

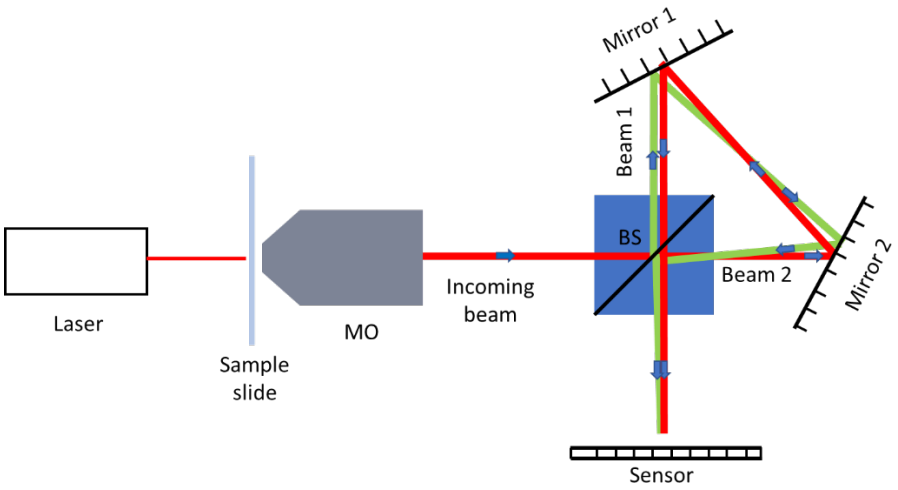

Fig 5.25 2D schematic of the common path self-referencing digital holographic microscope employing He-Ne laser and Sagnac interferometer

5.5.1.1 Calibration

Distribution of 15µm diameter polystyrene microspheres immersed in microscope oil is used for calibration of the microscope. Fig 5.26a shows a portion of the recorded object holograms. Recorded holograms are numerically processed which provides the object phase distribution shown in Fig 5.26b, which in turn will provide the object thickness distribution using the constant average RI of the microsphere and the microscope oil as shown in Fig. 5.26c and d.

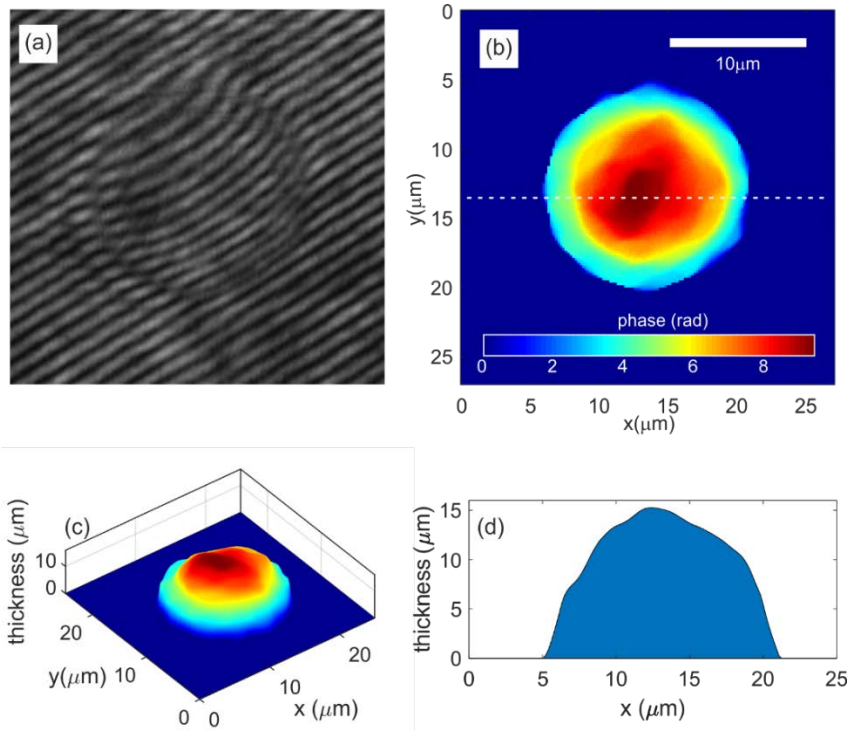

Fig 5.26 (a) recorded hologram of polystyrene beads (b) continuous phase distribution obtained after unwrapping (c) thickness distribution of the Polystyrene beads (d) line profile of the polystyrene bead

5.5.1.2 Imaging Red blood cells

To check the capability of the microscope for quantitative phase imaging of biological samples, thin smears of blood smear is imaged. Holograms are recorded at 10Hz for 30 seconds for numerical processing. Fig. 5.27a represents the object hologram in the case of blood sample. Numerical processing of the recorded holograms provides the continuous phase distribution of the object shown in Fig. 5.27b, which in turn provides the sample thickness profile shown in Fig. 5.27c and d.

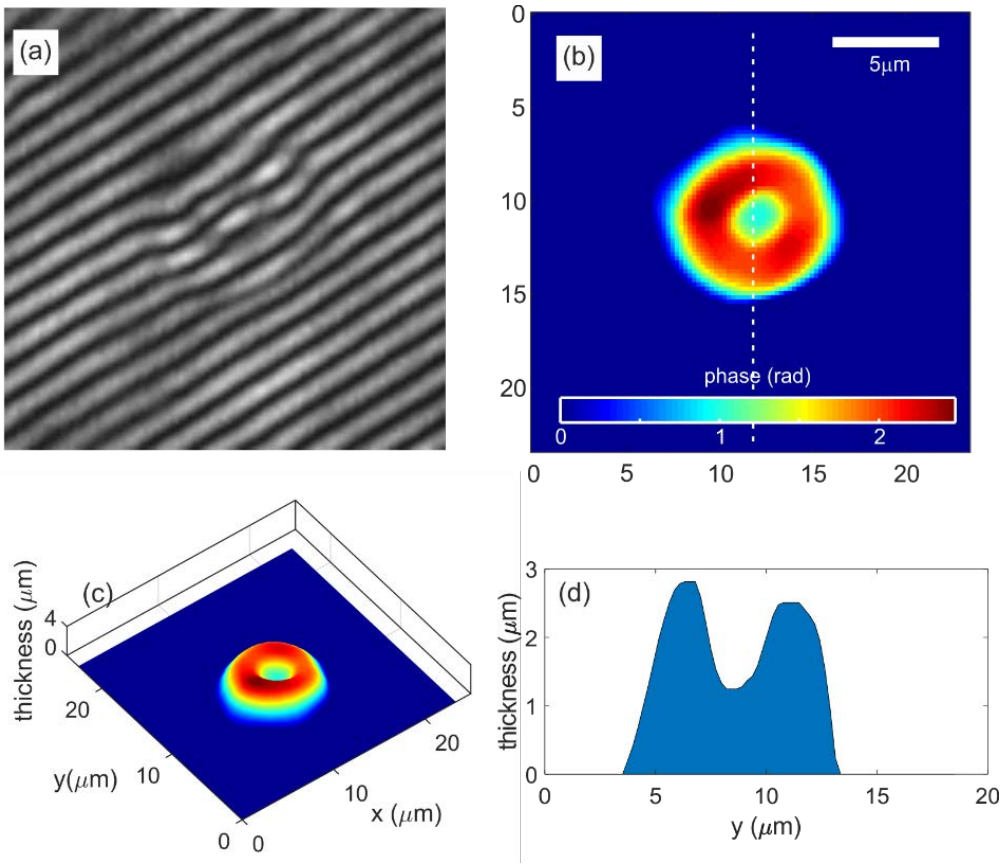

Fig 5.27 Quantitative phase imaging of human erythrocytes using He-Ne laser and Sagnac interferometer (a) recorded hologram (b) continuous phase distribution of the recorded RBCs (a) (c) 3D rendering of thickness distribution of RBCs inside the area of interest marked by white rectangle (d) cross sectional thickness profile of the RBC along the dashed line marked in Fig 5.27 (b)

5.5.2 Sagnac Digital Holographic Microscopy exploiting the coherence properties of LED

Sagnac interferometer has the inherent property of automatic optical path length matching of object and reference beams. This is ideal for generation of high contrast interference fringes using quasi-monochromatic LED. To investigate the use of low temporally coherent sources in generation of holograms and quantitative phase imaging, a digital holographic microscope employing Sagnac interferometer geometry, using an LED source (λ=627 nm, Luxeon star, max output power=2W, emitting area 1 mm^2) is constructed (Fig. 5.28). Here also the size of

the light emitting area of the LED is reduced with the help of 10x MO to increase the spatial coherence area of the source. Light from the real image of the LED illuminates the sample, which then passes through a MO (20x, 0.40NA). This beam is divided using a beam splitter and both the beams (transmitted and reflected) are then reflected using mirrors. After travelling in opposite directions, the two beams superpose at the exit face of the interferometer, generating holograms As the angle of the two mirrors are slightly different, the setup creates an off-axis geometry. The off-axis holograms are recorded with a CCD sensor (Thorlabs).

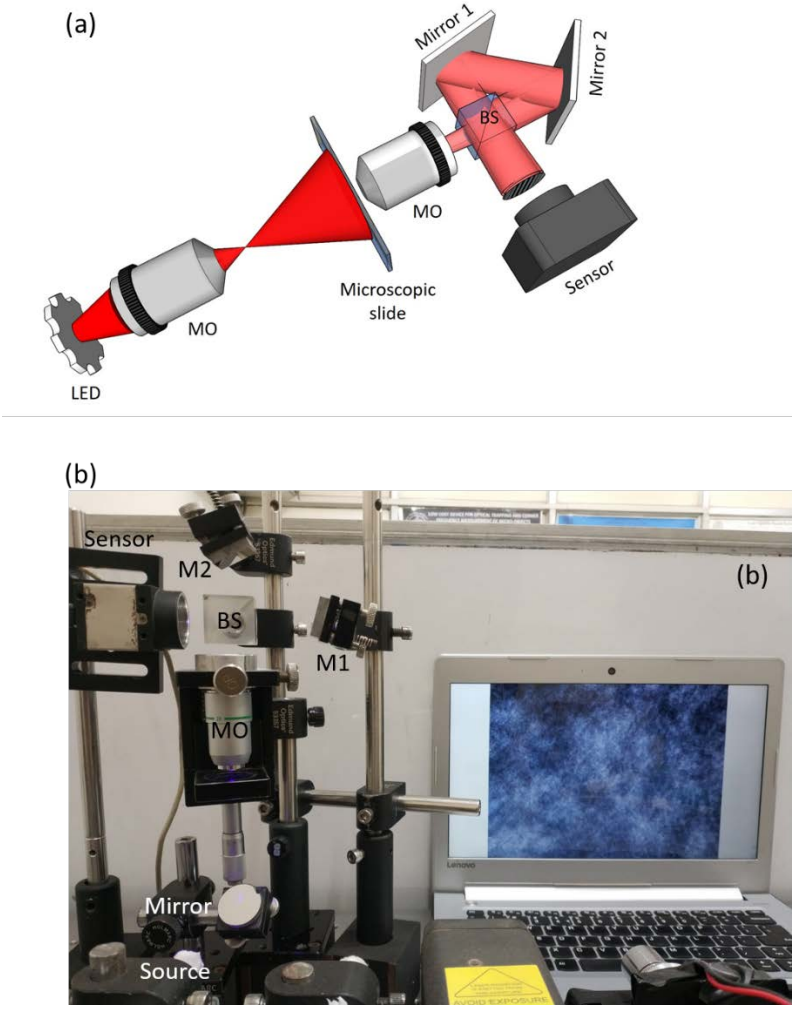

Fig 5.28 (a) shows the 3D schematic of the common path self-referencing digital holographic interference microscope employing Sagnac interferometer and LED (b) shows the table top setup in the laboratory

5.5.2.1 Temporal stability

As described in the previous sections temporal stability is quantified by recording a series of holograms for 30s at the rate of 30Hz. The mean of the standard deviation of time varying thickness profile quantifies the temporal stability of the setup. The path length variation over a period of 15s is measured to be 1.4 nm, which is slightly higher than other reported self-

referencing geometries. Fig 5.29 shows the histogram that represents the measured optical fluctuation at each spatial point (standard deviation of time varying thickness) in the FOV. The mean of these values represents the temporal stability of the microscope. Inset shows the time varying thickness at a spatial point in the FOV.

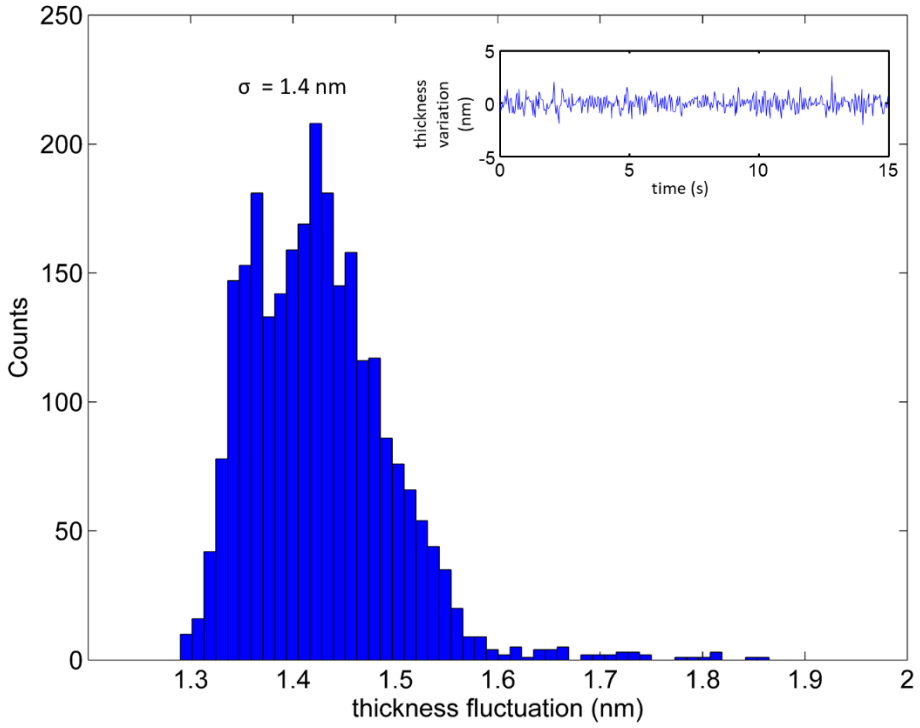

Fig 5.29 Temporal stability of the system. Histogram represents the measured counts for thickness fluctuation at each spatial point (standard deviation of time varying thickness). The mean of these values represents the temporal stability of the microscope. Inset shows the time varying thickness for a spatial point in the FOV.

5.5.2.2 Calibration

As in the case of other developed geometries, calibration of the microscope is carried out using 15µm diameter polystyrene microspheres immersed in microscope oil. Fig. 5.30a shows the object hologram in the case of microspheres. Digital holograms are numerically processed to extract the continuous phase distribution of the object (Fig. 5.30b), which in turn is used to determine the sample thickness profile (Fig. 5.30c and d)

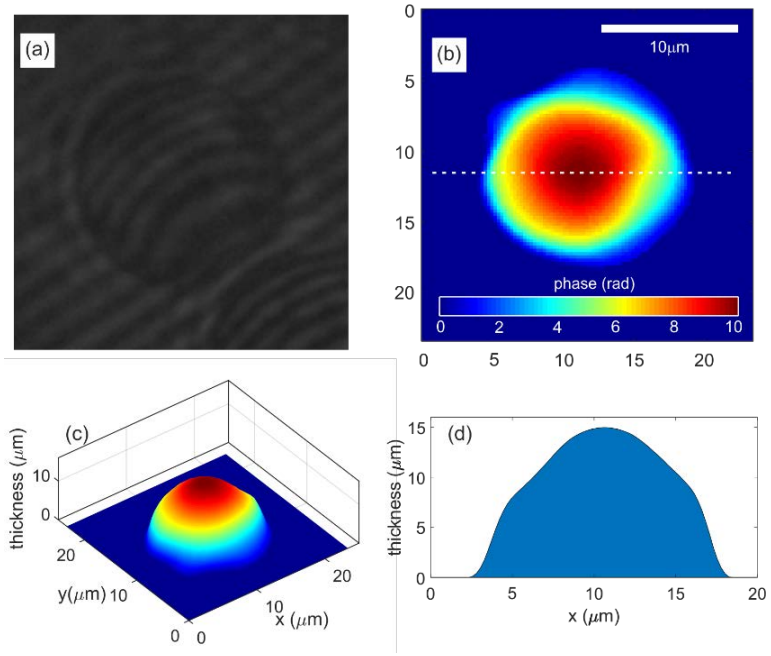

Fig 5.30 (a) recorded hologram of polystyrene beads (b) continuous phase distribution obtained after unwrapping (c) thickness distribution of the Polystyrene beads (d) line profile of the polystyrene bead

5.5.2.3 Imaging Red blood cells

To determine the ability of the microscope to quantify biological samples, thin blood smears are imaged using the developed geometry. Fig. 5.31a sows the object hologram in the case of thin blood smear. The reconstructed phase profile of the sample is shown in Fig. 5.31b, which in turn yields the thickness profile of red blood cells shown in Fig. 5.31c and 5.31d.

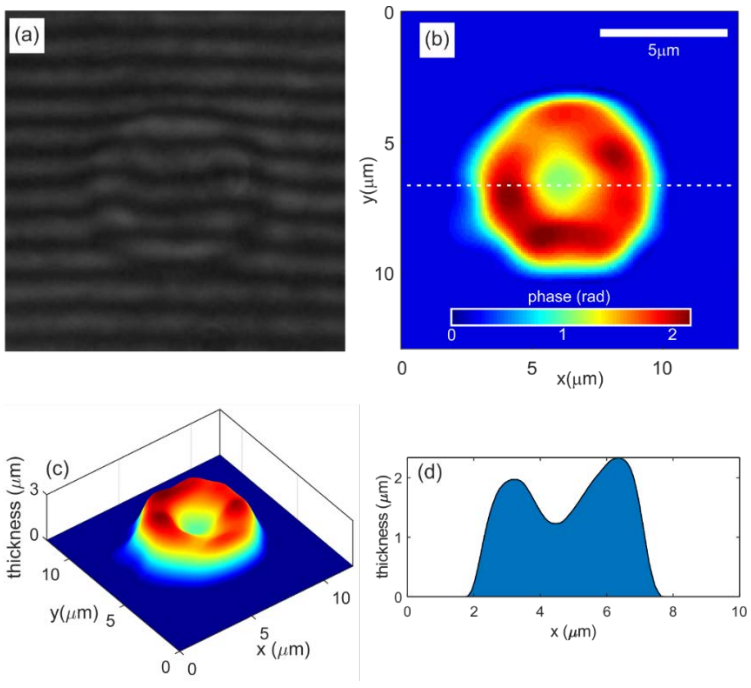

Fig 5.31 Quantitative phase imaging of human erythrocytes using LED and Sagnac interferometer (a) recorded hologram (b) continuous phase distribution of the recorded RBCs (c) 3D rendering of thickness distribution of RBC (d) cross sectional thickness profile of the RBC along the dashed line marked in Fig 5.31b.

5.6 Conclusion

From the techniques demonstrated in this chapter, it can be inferred that that large FOV, self-referencing, off-axis digital holographic phase contrast microscope can be constructed using LED sources by exploiting its coherence properties with the use of minimal optical components and hologram multiplexing. The low spatial coherence of the LED is enhanced by de-magnifying it (reducing its effective emitting area). The usable and effective FOV can be increased by using multiple self-referencing modules for hologram multiplexing (for example using a pair of parallelly placed Fresnel biprisms or employing two mirrors in the case of Lloyd's mirror interferometer). The increased FOV enables examination of large number of samples in a single shot. The use of LED also ensures that the spatial stability of the system improves compared to the system using a high coherent source. This leads to the conclusion that LED reduces the effects of the speckle noise as well as parasitic interference associated with high temporally coherent sources thereby enhancing the quality of the reconstructed phase profiles. The spatial stability of the digital holographic microscope employing LED sources is found to have improved by 2.5 times compared to the microscopes yielding laser sources. The temporal stability of the system employing Fresnel Biprism interferometer, Lloyd's mirror interferometer and Sagnac interferometer is found to be 0.9nm, 0.68nm and 1.4nm respectively. It can be concluded from these values that common path self-referencing geometries are more immune to the external mechanical vibrations thereby providing improved temporal stability compared to a two-beam geometry such as Mach Zehnder interferometer. Experiments have been conducted using a violet laser diode ((λ=405 nm, Thorlabs, maximum output power<2 mW) and CMOS sensor (Thorlabs, pixel pitch 2.2 μm) to explore

The developed devices can provide a multitude of bio-physical and bio-mechanical cell parameters based on the cell morphology and its time variation, which can be used for cell characterization and identification. Moreover, the simplicity of the arrangement makes the microscope easy to construct, requiring only few optical and imaging components compared to a two-beam geometry leading to small form factor. The table top microscopes employing Fresnel biprism and LED and Lloyd's mirror interferometer and laser have been converted into a portable, handheld module by incorporating off the shelf optical components and a 3D printed microscope frame. These low-cost, portable, stand-alone devices developed could be deployed in remote places where handy cell characterization devices are not easily available. The

portable devices make use of a DVD pickup lens for imaging which reduces the form factor of the device as well as its cost.